Indian Journal of Chemical Technology
Vol. 29, March 2022, pp. 139-148

Aluminium hydroxide impregnated sawdust adsorbent: An eco-friendly and low-cost strategy for defluoridation of water

Sujata Mandal*, Simmi Johri & Malarvizhi Govind

CLRI-Center for Analysis, Testing, Evaluation and Reporting Services (CATERS),
CSIR- Central Leather Research Institute, Adyar, Chennai 600 020, India

E-mail: sujata@clri.res.in, sujatamandal@rediffmail.com

Received 5 November 2021; accepted 5 January 2022

Environment-friendly and cost-effective adsorbent is necessary for removal of excess fluoride from water to control the spread of fluorosis among people in fluoride-rich area. Plant-based cellulosic materials are the preferred choice for this purpose. In this work, aluminium hydroxide impregnated sawdust (AHSD) adsorbent has been prepared, characterized and applied for defluoridation of water through batch and fixed-bed adsorption. Fluoride adsorption capacity of AHSD in batch adsorption experiment is 4.45 mg/g for the initial fluoride concentration between 5-50 mg/L. At low fluoride concentration, the Freundlich isotherm model fit reasonably well, while at higher fluoride concentration (> 40 mg/L) the Langmuir model show better fitting with the experimental data. The adsorption kinetics follow pseudo second-order kinetic model. In fixed-bed column adsorption, 4 g of the adsorbent is capable of bringing down the fluoride concentration from 5 mg/L to < 1.5 mg/L (WHO limit) for 690 mL of contaminated water. Residual aluminium in the treated water was within permissible limit of WHO. The reasonably good adsorption capacity and effectivity in both batch and fixed-bed column adsorption suggests that AHSD is an environment-friendly, cost-effective and promising adsorbent for defluoridation of water.

Keywords: Aluminium hydroxide, Batch adsorption, Fixed-bed column adsorption, Fluoride, sawdust

Fluoride is an important micronutrient for human beings however prolonged intake of high concentration of fluoride (more than 1.5 mg/L) can cause fluorosis. While moderate amounts of fluoride may cause dental fluorosis, long-term intake of large amounts of fluoride can lead to skeletal fluorosis, which is a potentially severe skeletal problem[1,2]. Fluorosis endemic has been reported by at-least 25 countries from all over the world[3]. Drinking water with high fluoride concentration is the primary source for fluoride to enter the human body. The WHO guideline value for fluoride in drinking-water is set at 1.5 mg/L[4]. Although the complete removal of fluoride is not desirable nevertheless, removal of excess fluoride from drinking water is necessary to avoid dental/skeletal fluorosis.

The existing techniques for the removal of fluoride from water are precipitation- coagulation, ion-exchange, membrane separation processes including reverse osmosis, nanofiltraton, dialysis, and adsorption[5,6]. All these techniques have both advantage and limitations. However, among all these techniques, adsorption is the most commonly used technique for drinking water treatment because of the simplicity of the technique, low operation cost and effective even at very low fluoride concentration in the water. Wide spectrum of natural and synthetic adsorbents has been experimented for the removal of fluoride from water[7-11]. Among all, alumina and aluminium-based minerals, compounds, (nano)-compositesand (nano)-materials have been found to be highly effective for this purpose[12-16]. A large number of low-cost adsorbents, primarily cellulosic materials fromplant/food wastes and their chemically modified forms have also been studied by several researchers[17-21] with an objective to create wealth from waste.However, development of potentially low-cost adsorbents by utilizing locally available materials is still in demandin order to design an affordable defluoridation technique. Among natural low-cost adsorbents, sawdust is a promising material for water/wastewater treatment due to its abundant availability and low-cost nature[22]. Literature reports are available on the use of raw/modified sawdust adsorbent for removal of heavy metal pollutants, arsenic[23] and dyes from water/wastewater by adsorption[24,25]. Moreover, to the best of ourknowledge, there are very limited report on fixed-bed column studies and no report on commercial plant using raw/modified sawdust adsorbent.

The objective of the present research was to utilize raw or modified plant-based cellulosic materials as low-cost adsorbent for defluoridation of water in domestic level as well as in community level set-up. With this objective, locally available sawdust has been chemically activated and tested for defluoridation studies. The present research article describes a systematic study on the development of the adsorbent, its characterization and application in removal of fluoride from water. Characterization techniques such as, elemental analyser, Fourier-Transform Infra-red spectroscopy (FTIR), X-ray diffraction (XRD), Scanning electron microscopy (SEM), BET surface area and porosity analysis, and thermo-gravimetric analysis (TGA), are used to study the morphological, chemical and thermal characteristics of the adsorbents. Adsorption equilibrium and kinetic studies are performed to check the fluoride adsorption efficiency of the developed adsorbent. Fluoride removal capacity of the adsorbent in fixed-bed column experiment has also been investigated.

Experimental Section

Chemicals

Aluminium nitrate nonahydrate[$Al(NO_3)_3.9H_2O$], sodium hydroxide (NaOH) pellets, and sodium fluoride (NaF) were procured from Merck Chemicals. Double distilled water was used for making standard solutions and in all the experiments.

Preparation of the adsorbent

Sawdust used in the present study was collected from three different saw mills located in Chennai, India, and it was mixture of different woods. The collected sawdust was dried under sunlight (40-42°C) for 2-3 days and then powdered in a mixer-grinder. The ground sawdust was sieved and particles of size less than 1mm were collected for further use. This mixture of raw sawdust is hereafter abbreviated as SD.

To prepare aluminium hydroxide impregnated sawdust (AHSD), 20g of the SD was added in 400 mL of 0.4M aluminium nitrate solution and kept at 60°C for 5 h, under continuous stirring. After 5 h, 2M NaOH solution was added very slowly to the aluminium nitrate soaked SD to make pH of the suspension between 8 and 9. The whole suspension was kept under stirring conditions for 30 min. The solid mass was separated, washed with water to remove any excess alkali followed by drying at 60°C in an air oven. The dry powder of the adsorbent thus obtained was named as AHSD and preserved in a closed container for further studies.

Characterization techniques

The elemental composition of the adsorbents was analysed using CHNS analyzer (ElementarVario Micro superuser, Germany). The FT-IR spectra were recorded in JASCO 4700 FTIR spectrometer by KBr pellet method. The X-ray diffractogram was taken in a Rigaku Miniflex Desktop XRD using CuK_{α} radiation. The morphology of the adsorbents was studied using scanning electron microscope (FEI Quanta 200 SEM). The thermal analyses were performed by Q50 TGA from TA Instruments, Austria, in the temperature between room temperature and 800°C with a ramp rate of 20°C/min and under N_2 atmosphere. The surface area and porosity of the adsorbents were measured at liquid nitrogen temperature using surface area and porosity analyser from BEL Inc. Japan, model: BelsorpMini X. Concentration of aluminium in the solution was analysed using Inductively Coupled Plasma-Optical Emission Spectrometer (ICP-OES, model: Prodigy XP from Teledyne Technologies Inc., USA). Zeta potential was measured in aqueous dispersion of the adsorbent using Litesizer 100, from Anton Paar GmbH. The concentration of fluoride ion in the solution was determined by ion-selective electrode method using 781 *p*H/Ionmeter (Metrohm, Switzerland) attached with fluoride ion-selective electrode (ISE).

Adsorption experiments

To study the removal of fluoride ions from aqueous solution by the developed adsorbents, adsorption experiments were performed in batches as well as in fixed-bed column modes.

Batch adsorption experiment

In a batch adsorption experiment, a fixed amount of the adsorbent was contacted with a known volume and predetermined concentration of the fluoride solution for a fixed time period and at constant temperature using a thermostatic water bath shaker (Model: SW23 from Julabo, Germany). After which the concentration of fluoride ion in the solution was determined by fluoride ISE in the presence of total ionic strength adjustment buffer (TISAB). TISAB solution was added to the analyte solution in 1:1 ratio (v/v). 100 mL of TISAB solution was prepared by dissolving 5.84 g NaCl, 5.75 mL glacial acetic acid and 0.45 g CDTA (trans-1,2-diamino-cyclohexane-

N,N,N,N-tetraacetic acid monohydrate) in de-ionized water at *p*H 5.5[26].

Optimization of contact time was performed by varying the contact time between 0 to 360 min keeping all other parameters (adsorbent dose, adsorbate volume and temperature) constant. To optimize the adsorbent dose, batch adsorption experiments were performed with varying adsorbent dose between 1 and 20 g/L while keeping all other parameters experimental parameters constant. To study the influence of solution *p*H, the *p*H of the fluoride solution was initially adjusted between 5 and 8 using dilute HCl (for *p*H<7) or dilute NaOH (for *p*H>7). Thereafter batch adsorption study was performed with 4 g/L adsorbent dose and 60 min contact time keeping all other parameters constant.

Adsorption equilibrium studies were performed with 4 g/L adsorbent dose, 60 min contact time, and initial fluoride concentration was varied between 5 and 50 mg/L keeping all other experimental parameters constant. After adsorption, concentrations of both fluoride and aluminium in the solution were determined.

Adsorption kinetic studies were performed with 4 g/L adsorbent dose, 60 min contact time, and the contact time was varied between 0 and 60 min keeping all other experimental parameters constant. Fluoride measurements were performed at various time intervals.

The adsorption capacity (mg/g) of the adsorbent was calculated by using the formula given below:

$$q_e = \frac{(C_o - C_e) \times v}{w \times 1000} \quad \ldots (1)$$

The percentage (%) of fluoride removed was calculated using the formula given below:

$$\text{Percentage Fluoride removed} = \frac{(C_0 - C_e)}{C_0} \times 100 \ldots (2)$$

where, q_e is the adsorption capacity at equilibrium (mg/g), C_0 is initial fluoride concentration (ppm), C_e is final fluoride concentration (ppm), w represents weight of the adsorbent (g), and v is the volume of fluoride solution (mL).

Fixed-bed column experiment

The experiment for the fixed-bed column study was performed in a glass column of length 50 cm and an inner diameter of 1.8 cm. The column was packed chronologically with glass beads, sand, adsorbent and again glass beads. The adsorbent bed height was 10 cm. Distilled water spiked with fluoride ions of predetermined concentration was allowed to flow through the vertically held fixed-bed packed column in an upward direction with a flow rate of 4-5 mL/min using a peristaltic pump. The solution coming out of the column was collected on a regular time interval and the concentration of fluoride was measured.

Results and Discussion

Characterization of the adsorbents

The elemental compositions of the SD and AHSD are determined and presented in Table 1. The carbon contents in both the adsorbents are very high (37-47%), as it is expected for plant-based natural materials. However, the carbon content in AHSD is less than that of SD due to aluminium hydroxide impregnation in AHSD. At the same time, the percentage of nitrogen in the AHSD is more than that of SD, which may be due to the fact that nitrate salt of aluminium has been used to prepare AHSD. No sulphur has been detected in both the adsorbents. Zeta potential of the SD and AHSD are found to be -18.4 and 14.3 mV respectively. This indicates that impregnation of $Al(OH)_3$ introduces positive charge to the adsorbent.

Figure 1 shows the SEM images of SD and AHSD under different magnifications (10 and 20 μm). The SEM images of the untreated sawdust (SD) clearly show the fibrous structure with cracks in it. The deposition of aluminium hydroxide particles on the surface of sawdust as well as in the pores and cracks are clearly seen in the SEM images of AHSD.

The FTIR spectra of SD and AHSD presented in Fig. 2a clearly shows all the characteristic absorptions

Table 1 — Elemental composition of the SD and AHSD.

Name of the adsorbent	N (%)	C (%)	H (%)	S (%)	O (%)	Al (%)[¥]
SD	4.59	46.67	6.52	BDL	38.13	BDL
AHSD	6.76	37.61	4.45	BDL	49.48	4.59

[#]BDL: below detection limit, [¥]Obtained by ICP analysis

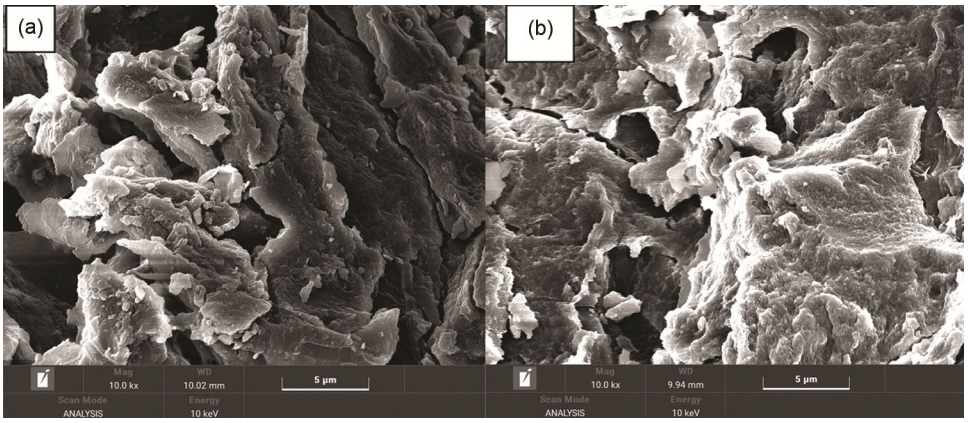

Fig. 1 — Scanning electron microscopic (SEM) images of the (a) SD and (b) AHSD.

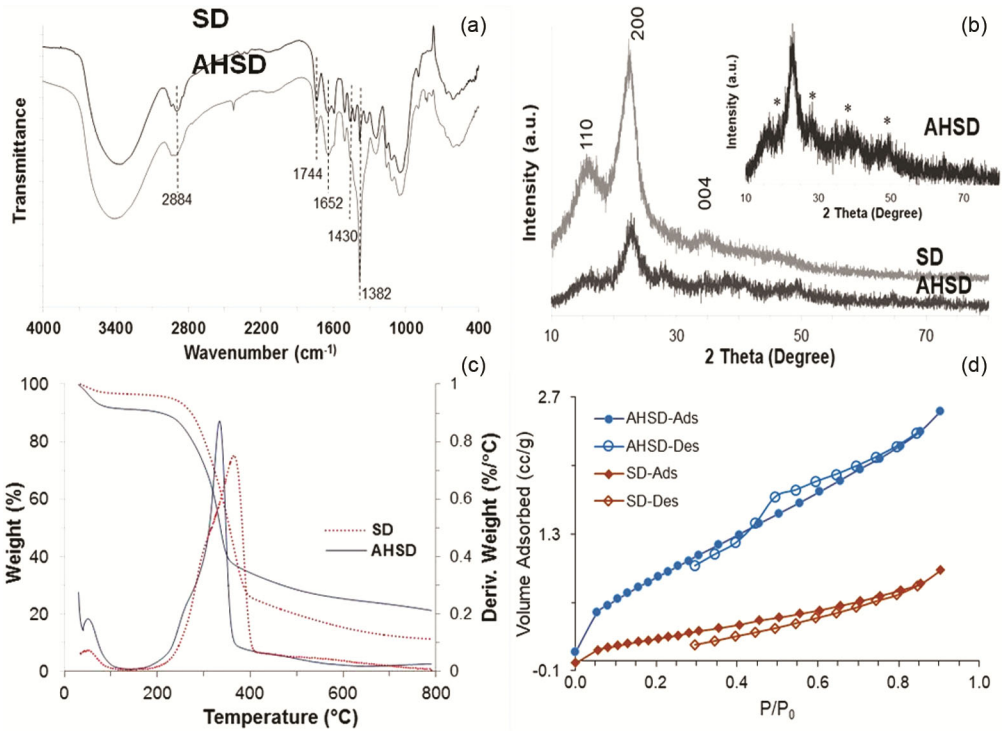

Fig. 2 — (a) FTIR spectra, (b) XRD patterns, (c) TGA-DTG thermograms and (d) N_2 adsorption-desorption isotherms of SD and AHSD.

of cellulose crystals, including the O–H stretching vibration between 3650-3000 cm^{-1}, C–H stretching vibration between 2950-2850 cm^{-1}, the bending of –C-6–CH_2– vibration at 1430 cm^{-1} and the deformation, wagging, and twisting modes of the anhydroglucopyranose units in the 1800-600 cm^{-1} wavenumber range[27]. The sharp shoulder peak at 1744 cm^{-1} may be attributed to the C=O stretching vibration, and it is also the characteristic wave peak for hemicellulose. The vibration peaks at 2945 cm^{-1} and 1751 cm^{-1} weakened in AHSD, which indicated that the amounts of hydroxyl, hemicellulose, and cellulose reduced with the process of treatment. The absorption band for O-H group stretching vibration is observed at 1652 cm^{-1} wavenumber[28]. The band between 1200 and 950 cm^{-1} is attributed to the C–O stretching vibration characteristic of the carbohydrates. The only difference in the FTIR spectrum of SD and AHSD is the presence of very strong and sharp peak at 1382 cm^{-1} in AHSD. In the spectrum of SD, the low intense peak at 1382 cm^{-1} is attributed to the overlapping of C-H bending and CH_3 deformation vibrations[29], while the same absorption band but of strong intensity in AHSD is due to the combination of vibration from CH_3 bending and anti symmetric stretching vibration of nitrate ions[30].

The XRD patterns presented in Fig. 2b shows prominent peaks at 2θ positions 16.2, 22.9 and 34.5 degrees which were assigned to the 110, 200 and 004 planes of cellulose crystal, respectively[31,32]. Diffraction peaks corresponding to the gibbsite phase of $Al(OH)_3$ phase has been marked (*) in the X-ray diffractogram of AHSD[33] presented in the inset of Fig. 2b. The characteristic diffraction peaks for 010 and 110 planes of $Al(OH)_3$ appears at 2θ positions between 18-21 degree[34,35] possibly been overlapped by the broad peaks of cellulose.

The TGA profile of SD and AHSD presented in Fig. 2c show similar pattern and match well to that of the cellulose. The maximum weight loss takes place nearly at 360 and 330°C for the SD and AHSD respectively. A similar observation has been reported by Wu et al. (2017) for Al-based nanoparticle impregnated saw-dust[36]. In comparing the TGA-DTG profiles of SD and AHSD, the higher weight loss below 110 °C for AHSD indicates higher moisture content in AHSD as compared to SD. The final residue remained after 800°C for SD and AHSD are 11.32 and 21.23%, respectively. The organic content (weight loss between 230 and 400°C) in the SD and AHSD is nearly 70 and 54% respectively. The less weight loss in AHSD is partially due to the impregnated aluminium hydroxide in it and also due to the loss of volatile and washable matter during the chemical impregnation process.

The N_2 adsorption-desorption isotherms of the SD and AHSD are presented in Fig. 2d. The specific surface area of SD and AHSD obtained from BET model are 1.11 and 3.61 m^2/g, respectively. Total pore volume of SD and AHSD are 1.44×10^{-3} and 3.95×10^{-3} cc/g with average pore diameter being 5.19 and 4.38 nm respectively. The monolayer adsorption capacity of the two adsorbents are 0.25 and 0.83 cc/g for SD and AHSD respectively. As compared to SD, the surface area and pore characteristics of AHSD increased by more than 3-fold indicating better adsorption property of the AHSD.

Batch adsorption studies

Influence of aluminium hydroxide impregnation

The fluoride adsorption capacities of the SD and AHSD at different fluoride concentrations is presented in Fig. 3. The aluminium hydroxide impregnated sawdust (AHSD) showed very high fluoride adsorption capacity as compared to the raw sawdust (SD). The increase in fluoride adsorption capacity of AHSD is due to the following factors:

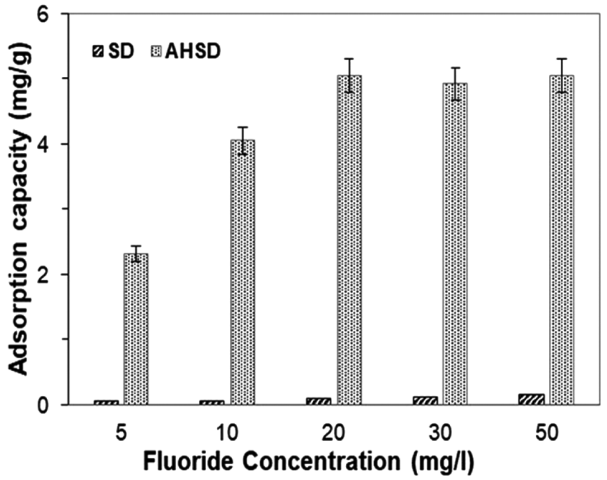

Fig. 3 — Fluoride adsorption capacity of the SD and AHSD at different fluoride concentrations (adsorbent dose: 2 g/L, adsorbate volume: 50 mL, contact time: 60 min).

- the positive surface charge that promotes adsorption of fluoride anion.
- the high specific surface area.
- dispersion of $Al(OH)_3$ on the sawdust improved availability of adsorption sites.

Since the fluoride adsorption capacity of SD is negligible as compared to the AHSD, detailed adsorption studies are performed only with AHSD.

Influence of operational parameters

Influence of operational parameters for batch adsorption studies, such as contact time, adsorbent dose, and solution *p*H were optimized for maximum adsorption, and the data are presented in Fig. 4 (a-c). Figure 4a shows that the maximum fluoride adsorption occurred at 60 min and further increase in contact time does not improve the fluoride adsorption. The adsorption dose variation data presented in Fig. 4b shows that there is sharp increase in fluoride adsorption from 39.9% to 93.2% on increasing the adsorbent dose from 1 to 4 g/L. After 4 g/L adsorbent dose, there is very slow increase in adsorption and 99.1% fluoride is adsorbed with an adsorbent dose of 10 g/L. The influence of solution *p*H on fluoride adsorption by AHSD is presented in Fig. 4c. It shows that the adsorption of fluoride on AHSD is not significantly affected by the solution *p*H between 6.0 to 6.5, however there is decrease in fluoride adsorption at a solution *p*H>8. The decrease in fluoride adsorption in alkaline *p*H might be due to the increase in concentration of the competing hydroxyl (OH^-) ions Therefore, further experiments on fluoride adsorption on AHSD are performed at the

normal *p*H of the fluoride solution, which lies between 6.4-6.5.

Adsorption equilibrium

The fluoride adsorption capacity and percentage adsorption of AHSD over a range of initial fluoride concentration has been plotted as a function of equilibrium fluoride concentration and presented in Fig. 5a. The adsorption capacity value increases and the percentage adsorption decreases with increase in initial fluoride concentration in the solution. The maximum fluoride adsorption capacity achieved by the adsorbent is 4.45 mg/g at an initial fluoride concentration of 40 mg/L. It is possible to achieve ~100% removal of fluoride from water by increasing the adsorbent dose, however low concentration (< 1.5 mg/L) of fluoride in water is recommended for its micronutrient value. An adsorbent dose of 4 g/L is capable of bringing down the fluoride concentration in water from 10 mg/L to a concentration within the acceptable limit set by WHO, within 60 min of contact.

In order to find out the leaching of aluminium from the AHSD adsorbent to the water during fluoride adsorption, the solutions after fluoride adsorption studies were tested for residual aluminium and the values are presented in the Fig. 5b. In 5 and

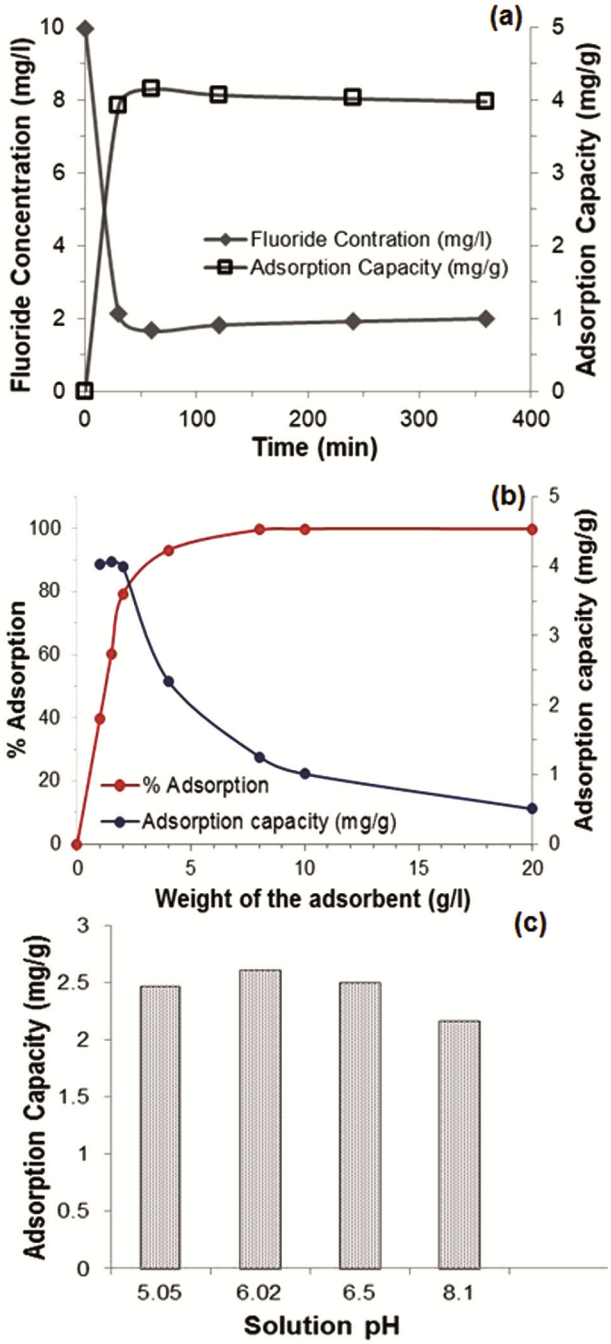

Fig. 4 — Adsorption of fluoride by AHSD as a function of (a) contact time, (b) adsorbent dose, and (c) solution pH (initial fluoride concentration: 10 mg/l; adsorbate vol.: 50 ml; Temp: 28 °C; adsorbent dose: 2 g/l (a), 4 g/l (c); contact time (b.c): 60 min).

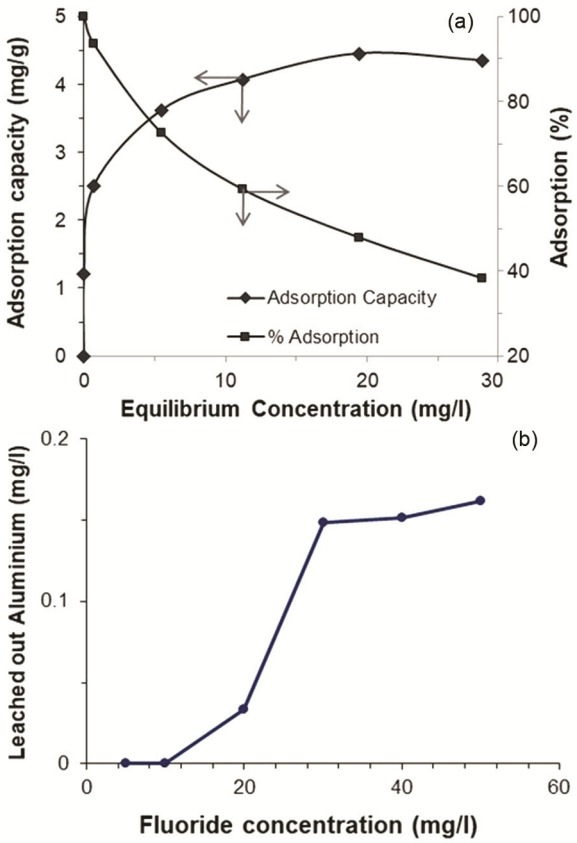

Fig. 5(a) — Fluoride adsorption equilibrium of AHSD, and (b) aluminium leaching from the AHSD as a function of initial fluoride concentration (initial fluoride concentration: 5-50 mg/l, adsorbent dose: 4 g/L, contact time: 60 min, temperature: 28 ºC).

10 mg/L fluoride solution, the residual aluminium has been found to be below the detection limit of ICP. In general, solubility of aluminium in water increases in presence of high fluoride concentrations due to the formation of soluble monomeric aluminium fluoride and aluminium hydroxyl fluoride complexes[37]. However, residual aluminium concentration in 20–50 mg/L fluoride solution after 60 min of adsorption was well below 0.2 mg/L.

The adsorption equilibrium data obtained for the adsorption of fluoride on AHSD were fitted to the standard Langmuir and Freundlich adsorption isotherm models. The form of the Langmuir[38] and the Freundlich[39] isotherm models used in the present study are given as equation 3 and equation 4, respectively.

$$\frac{C_e}{q_e} = \frac{1}{bV_m} + \frac{C_e}{V_m} \quad \ldots (3)$$

$$\ln q_e = \ln k + \frac{1}{n} \ln C_e \quad \ldots (4)$$

where, C_e and q_e has the same meaning as described earlier; V_m and b are the Langmuir isotherm constants representing monolayer adsorption capacity and adsorption bond energy respectively, k and n are the Freundlich isotherm constants representing adsorption capacity and intensity of adsorption respectively. The values of b and V_m were calculated from the slope and intercept of the plot of C_e/q_e versus C_e. The values of k and n were calculated from the slope and intercept of the plot of $\ln(q_e)$ versus $\ln(C_e)$.

Values of equilibrium adsorption capacity for each isotherm model were calculated from the values of isotherm constants and equilibrium concentrations, and the respective isotherm equation. Figure 6 shows the plots of equilibrium adsorption capacity, experimental and calculated using the isotherm models, as a function of equilibrium fluoride concentration. The values of isotherm constants are presented in the inset of Fig. 6. The values of correlation coefficient (R^2) for both the models are very close to 'one', which indicates excellent fitting of both the Langmuir and Freundlich isotherm models with the experimental data. However, at low fluoride concentration, the Freundlich isotherm model fitted reasonably well with the experimental data while at higher fluoride concentration (> 40 mg/L) the Langmuir model shows better fitting with the experimental data. Gamvir and Das (2011) also reported that the Freundlich adsorption isotherm

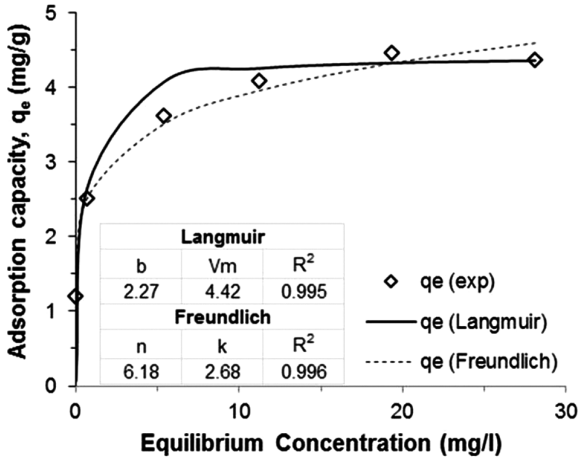

Fig. 6 — Fluoride adsorption isotherm of AHSD (the data points represent experimental values, solid line represents the Langmuir and the dotted line represents the Freundlich isotherm models).

model is the suitable model for adsorption of fluoride ions (initial fluoride concentration 10-60 mg/L) on the aluminium coated rice husk ash adsorbent[21]. The value of Freundlich constant 'n' (>1) represents good adsorption characteristics[40] of AHSD for the adsorption of fluoride ions in aqueous medium.

The fluoride adsorption capacity of the aluminium hydroxide impregnated sawdust (AHSD) adsorbent and various raw/modified bio-based adsorbents reported in the literature in last ten years, are presented in Table 2. The values presented in Table 2 show that except few, the defluoridation capacity of AHSD is comparable with other raw/modified bio-based adsorbents reported in the literature. Although the Zr-modified Grape pomace adsorbent also reported to show high defluoridation capacity but the study has been performed at very high fluoride concentrations (> 1000 mg/L) and needs *p*H adjustment for the adsorption[18]. Therefore, the case of Zr-modified Grape pomace adsorbent cannot be compared with the AHSD adsorbent from the present study.

Adsorption kinetics

Figure 7a shows the change in fluoride ion concentration and fluoride adsorption percentage by the AHSD as a function of time. It is clear from the Figure 7a that the adsorption of fluoride on AHSD is very fast, 50% of the adsorption is reached in one min and the maximum adsorption is achieved within 60 min of contact. Mondal *et al*. (2015) also reported that the equilibrium adsorption of fluoride took place in 60 min when aluminium impregnated coconut fiber was used as adsorbent[20]. The adsorption kinetic data are fitted to the pseudo-second order kinetic model.

Table 2 — Fluoride adsorption capacities of various raw/modified biosorbents.

Sl. No.	Adsorbent	Adsorption capacity (mg/g)	Initial fluoride concentration (mg/L)	Contact time (min)	Reference
1.	Zr-modified Grape pomace	7.5 (*p*H 3)	10-1000	60	[18]
2.	Fe(III)-loaded sisal fibre	0.4	--	60	[9]
3.	*Ficus benghalensis* leaf	2.24	2-25	90	[10]
4.	Raw wheat straw	3.1	2.5 - 15	75	[41]
5.	Raw Sawdust	1.93	2.5 - 15	75	[41]
6.	Ca^{2+}impregnated banana peel dust	17.4-39.5 (Langmuir model)	1.5 - 20	60	[42]
7.	Tea leaves	0.25	5-15	150	[43]
8.	Zirconium modified tea waste	20.56	5-400	90	[19]
9.	Anionic polyacrylamide mediated tea waste supported hydrous aluminium oxide	42.14	5-200	180	[44]
10.	Al loaded coconut fiber	3.2	1-10	--	[20]
11.	Surface modified *Adansonia digitata* fruit pericarps	0.23-0.44 (Langmuir model)	5-50	24 h	[45]
12.	Aluminium hydroxide impregnated sawdust (AHSD)	4.45	5-50	60	Present study

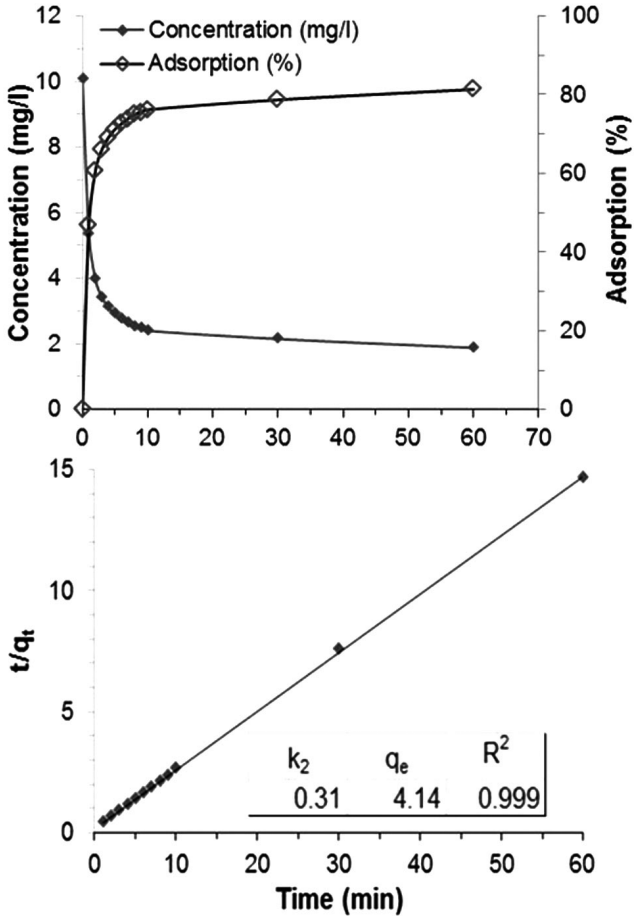

Fig. 7— (a) Change in fluoride ions concentration and percentage adsorption as a function of time (vol. of fluoride solution: 50 mL, adsorbent dose: 2 g/L, initial fluoride concentration: 10 mg/L, temperature: 28ºC) and (b) pseudo-second order kinetic plot, for fluoride adsorption on AHSD.

The linearized equation of the kinetic model as proposed by Ho and Mckay (2002)[46] is presented as equation 5.

$$\frac{t}{q_t} = \frac{t}{qe} + \frac{1}{k_2.q_e^2} \quad ...(5)$$

where, t is time (min), q_e and q_t are the adsorption capacity at equilibrium and at time t (mg/g), k_2 is the pseudo-second order rate constant [g/(mg.min)].

Figure 7b shows the pseudo-second order kinetic plot and the values of kinetic parameters. The value of pseudo-second order rate constant is 0.31 g/(mg.min). The value of equilibrium adsorption capacity calculated using the kinetic model (4.14 mg/g) matches well with the experimental value (4.12 mg/g). The excellent fitting of the pseudo second-order kinetic model as confirmed by the value of correlation coefficient (R^2= 0.999) implies that pseudo second-order kinetic model is the appropriate model to describe the kinetic behaviour of fluoride adsorption on AHSD. The suitability of pseudo-second order kinetic model for the adsorption of fluoride ions by aluminium hydroxide coated rice husk ash has been reported by Ganvir and Das (2011)[21].

Fixed bed column studies

The glass column was vertically fixed on a stand and packed with the adsorbent AHSD and other materials as described in section 2.4.2. The schematic diagram of the fixed-bed column set-up

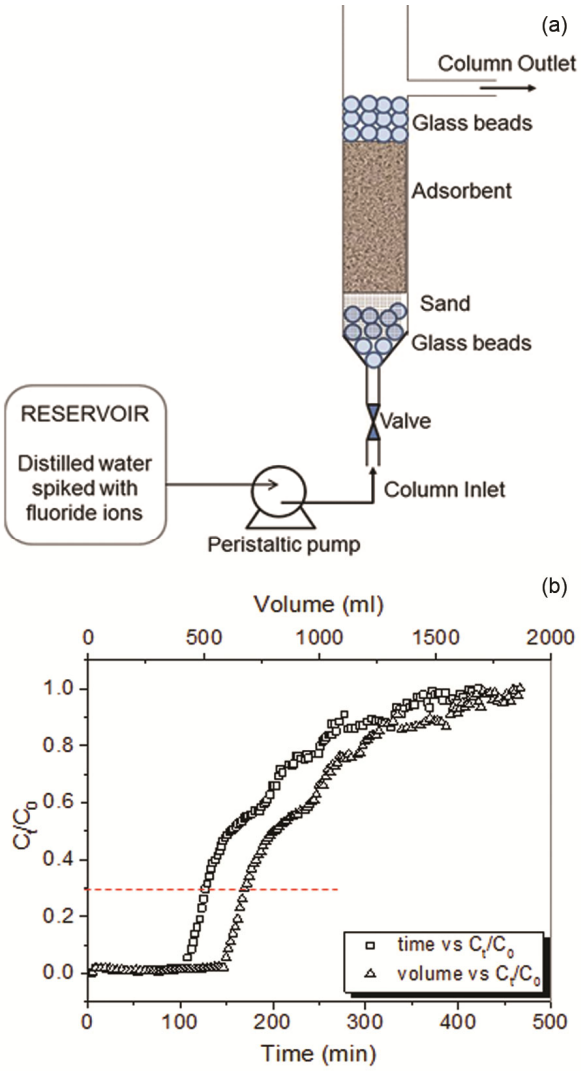

Fig. 8 — (a) Schematic diagram of the fixed-bed column set-up, and (b) Break though curve of fluoride adsorption on AASD as a function of time and volume of water passing through the column (initial fluoride concentration: 5 mg/L, adsorbent bed height: 10 cm, adsorbent weight: 4 g, flow rate: 4 mL/min, temp: 28ºC).

has been shown in Fig. 8a. Distilled water spiked with 5 mg/L of fluoride was pumped through the packed column in an upward direction with a flow rate of 4 mL/min using a peristaltic pump. The treated water was collected from the outlet at regular intervals and the concentration of fluoride was measured.

The AHSD adsorbent performed very well in the fixed-bed column experiment. Figure 8b shows the breakthrough curves as a function of time and as a function of volume of fluoride solution passing through the column. The point where the fluoride concentration of the treated water reached the WHO set limit of 1.5 mg/L is considered as the point of column exhaustion. Thus, ~690 mL of fluoride contaminated water has been considered as treated till the column gets exhausted although a total of 1620 mL of water was passed through the column till C_t/C_0 = 1 (or $C_t = C_0$). Therefore, 4 g of the AHSD adsorbent is capable of bringing down the fluoride concentration from 5 mg/L to < 1.5 mg/L for 690 mL of fluoride contaminated water.

Conclusion

Aluminium hydroxide impregnated sawdust (AHSD) adsorbent has been prepared, characterized and effectively used as adsorbent for defluoridation of water through batch and fixed-bed column adsorption processes. Fluoride adsorption capacity of the adsorbent is 4.45 mg/g at the normal *p*H of the water. At low fluoride concentration, the adsorption isotherm data fits well to the Freundlich isotherm model confirming multilayer adsorption. The rate of adsorption is rapid for initial 10 min. The fluoride adsorption kinetics follow the pseudo-second order kinetic model. The developed adsorbent could effectively remove fluoride from water both in batch as well as in fixed-bed adsorption mode. In fixed-bed column process, a column packed with 4 g of the AHSD is capable of treating 690 ml of 5 mg/l fluoride spiked water to below the WHO maximum permissible limit (1.5 mg/L). Therefore, it may be concluded that the AHSD adsorbent made from waste sawdust, is an eco-friendly, low-cost and promising adsorbent for defluoridation of water.

Acknowledgement

Authors wish to acknowledge the financial support received from CSIR-CLRI. SJ thanks the Director, CSIR-CLRI, for support and encouragement. CSIR-CLRI communication no. 1465.

Disclosure statement

No potential conflict of interest was reported by the authors.

References

1 World Health Organization (WHO), Geneva, Switzerland. Fluorides, Environmental Health Criteria No. 227, (2002).
2 Srivastava S & Flora S J S, *Curr Environ Health Rep*, 7 (2020) 140.
3 World Health Organization (WHO), Guidelines for Drinking-Water Quality: Incorporating First Addendum Recommendations, 3rd ed., World Health Organization, 20 Avenue Appia, 1211 Geneva 27, Switzerland, 1 (2006) 375.

4 World Health Organization (WHO), Guidelines for Drinking-Water Quality. Recommendations. 3rd edition, World Health Organization, Geneva, 1 (2004).
5 Mandal S &Mayadevi S, *Fluoride: Properties, Applications and Environmental management* edited by S D Monroy, Nova Science Publishers, Inc. New York, (2011) 159.
6 He J, Yang Y, Wu Z, Xie C, Zhang K, Kong L & Liu J, *J Environ. Chem Eng*, 8 (2020) 104516.
7 Wei L, Zeitzschmann F, Rietveld L C & Halem D V, *J Water Process Eng*, 40 (2021) 101957.
8 Saini A, Maheswari P H, Tripathy S S, Waseem S & Dhakate S R, *J Water Process Eng*, 34 (2020) 101136.
9 Mwakabona H T, Mlay H R, Van der Bruggen B & Njau K N, *J Hazard Mater*, 362 (2019) 99.
10 George A M & Tembhurkar A R, *Sust Chem Pharm*, 10 (2018) 125.
11 Dewage N B, Liyanage A S, Pittman Jr C U, Mohan D & Mlsna T, *Bioresour Technol*, 263 (2018) 258.
12 Samrat M V V N, Gandhi K S, Rao K K & Bhattacharyya S, *J Environ Chem Eng*, 8 (2020) 103934.
13 Wang Q, Chen P, Zeng X, Jiang H, Meng F, Li X, Wang T, Zeng G, Liu L, Shu H& Luo X, *J Hazard Mater* 381 (2020) 120954.
14 Barik B, Nayak P S, Satish L, Achary K, Kumar A & Dash P, *New J Chem*, 44 (2020) 322.
15 Mahfoudhi N & Boufi S, *J Environ Chem Eng*, 8 (2020) 103779.
16 Mandal S & Mayadevi S, *Chemosphere*, 72 (2008) 995.
17 Wang D, *Cellulose*, 26 (2019) 687.
18 Zhang Y & Huang K, *RSC Adv*, 9 (2019) 7767.
19 MeiL, Peng C, Qiao H, Ke F, Liang J, Hou R, Wan X & Cai H, *RSC Adv*, 9 (2019) 33345.
20 Mondal N K, Bhaumik R and Datta J K, *Alex Eng J*, 54 (2015) 1273.
21 Gamvir V & Das K, *J Hazard Mater*, 185 (2011) 1287.
22 Hashem A, Elhmmali M M, Hussein H A & Senousi M A, *Polym Plast Technol Eng*, 45 (2006) 821.
23 Setyono D & Valiyaveettil S, *ACS Sust Chem Eng*, 2 (2014) 2722.
24 Benyoucef A, Harrache D, Djaroud S, Sail K, Mateu D G & Guardia M D L, *Cellulose*, 27 (2020) 8169.
25 Sahmoune M N & Yeddou A R, *Desalin Water Treat*, 57 (2016) 24019.
26 Mandal S & Mayadevi S, *J Hazard Mater*, 167 (2009) 873.
27 Lu P & Hsieh Y L, *Carbohydr Polym,* 87 (2012) 2546.
28 Barrera A P, Marquez O G M, Revilla G O & Velazquez T G, *CyTA J Food* 12 (2014) 65.
29 Saha T K, Biswas R K, Karmakar S & Islam Z, *ACS Omega,* 5 (2020) 13358.
30 Mandal S, Natarajan S, Suresh S, Chandrasekar R, Jothi G, Muralidharan C & Mandal A B, *Appl Clay Sci* 115 (2015) 17.
31 Prakash R, Mandal S & Bheeter S R, *J Water Process Eng*, 35 (2020) 101208.
32 Nie K, Sang Y, Liu S, Han G, Ben H, Ragauskas A J & Jiang W, *Polymers*, 11 (2019) 907.
33 Yang J & Frost R L, *Int J InorgChem*, 2008, 602198.
34 Madej D & Tyrała K, *Mater*,13 (2020) 1403.
35 Mahinroosta M & Allahverdi A, *Int Nano Lett*, 8 (2018) 255.
36 Wu K, Liu T, Lei C & Zhang F, *Environ ProgSust Energy*, 36 (2017) 1314.
37 George S, Pandit P & Gupta A B, *Water Res*, 44 (2010) 3055.
38 Langmuir I, *J Am Chem Soc*, 40 (1918) 13.
39 Freundlich H, *Z Phys Chem*, 57 (1906) 385.
40 Treybal R E, *Mass Transfer Operations*, 3rd edition, McGraw-Hill Book Company, Singapore, (1981) 590.
41 Yadava A K, Abbassi R, Gupta A & Dadashzadeh M, *Ecol Eng*, 52 (2013) 211.
42 Bhaumik R & Mondal N K, *Appl Water Sci*, 6 (2016) 115.
43 Jenish S & Methodis P A, *Asian J Chem*, 23 (2011) 2889.
44 Cai H, Chen G, Peng C, Xu L, Zhu X, Zhang Z, Dong Y, Shang G, Ke F, Gao H & Wan X, *RSC Adv*, 5 (2015) 29266.
45 Mihayo D, Vegi M R & Vuai S A H, *J Dispers Sci Technol*, under publication.
46 Ho Y S & McKay G, *Adsorp Sci Technol*, 20 (2002) 797.